

Dataset-Free Weight-Initialization on Restricted Boltzmann Machine

Muneki Yasuda*

Ryosuke Maeno†

Chako Takahashi*

Abstract

In feed-forward neural networks, dataset-free weight-initialization method such as LeCun, Xavier (or Glorot), and He initializations have been developed. These methods randomly determine the initial values of weight parameters based on specific distributions (e.g., Gaussian or uniform distributions) without using training datasets. To the best of the authors' knowledge, such a dataset-free weight-initialization method is yet to be developed for restricted Boltzmann machines (RBMs), which are probabilistic neural networks consisting of two layers. In this study, we derive a dataset-free weight-initialization method for Bernoulli–Bernoulli RBMs based on a statistical mechanical analysis. In the proposed weight-initialization method, the weight parameters are drawn from a Gaussian distribution with zero mean. The standard deviation of the Gaussian distribution is optimized based on our hypothesis which is that a standard deviation providing a larger layer correlation (LC) between the two layers improves the learning efficiency. The expression of the LC is derived based on a statistical mechanical analysis. The optimal value of the standard deviation corresponds to the maximum point of the LC. The proposed weight-initialization method is identical to Xavier initialization in a specific case (i.e., in the case the sizes of the two layers are the same, the random variables of the layers are $\{-1, 1\}$ -binary, and all bias parameters are zero).

1 Introduction

A restricted Boltzmann machine (RBM) is a probabilistic neural network defined on a bipartite undirected graph consisting of two layers: visible and hidden layers [1, 2]. The visible layer consists of visible variables that directly correspond to the data points, whereas the hidden layer comprising hidden variables does not, wherein both visible and hidden variables are random variables. The hidden layer creates complex correlations among the visible variables. The RBMs have a wide range of applications, such as collaborating filtering [3], dimensionality reduction [4, 5], classification [6, 7], anomaly detection [8, 9], and deep learning [10, 11, 12]. Further, the RBMs have been actively investigated in the fields of statistical mechanics [13, 14, 15, 16].

Learning parameters in gradient-based successive learning for a model are initialized using some approach, and the initialization approach can affect the learning result. Therefore, selecting an appropriate initialization approach is essential. Finding an universal optimal-initialization approach can be challenging because the optimal initialization strongly depends on a given dataset, and ultimately, the optimal initial values are the learning solution. An initialization method that is dataset free and stably provides good learning solutions is useful. Such useful weight-initialization methods exist for (non probabilistic) feed-forward neural networks, e.g., LeCun [17], Xavier (or Glorot) [18], and He [19] initializations, wherein the weight parameters of the feed-forward neural network are initialized by small random values drawn

*Graduate School of Science and Engineering, Yamagata University

†Techno Provide Inc.

from a specific distribution (and its bias parameters are usually initialized to zero). These three weight-initialization methods depend only on the structure of the network. However, such a weight-initialization method does not exist in RBM learning.

This study investigates a dataset-free weight-initialization method for Bernoulli–Bernoulli RBMs whose the visible variables are $\{-1, 1\}$ -binary and the hidden variables are $\{0, 1\}$ - or $\{-1, 1\}$ -binary. In the proposed weight-initialization method, the bias parameters are initialized by a fixed value and the weight parameters are initialized by small random values drawn from a specific distribution, similar to the aforementioned weight-initialization methods for feed-forward neural networks. Wherein the distribution generating initial weights is assumed to be a Gaussian distribution with zero mean and standard deviation σ . The value of σ is determined by a criterion based on the hypothesis that a σ value providing a larger layer correlation (LC) between the visible and hidden layers (i.e., a statistical average of covariance between the two layers) improves the learning efficiency. The learning efficiency mentioned here is considered as the growth rate of the training likelihood.

In section 3, the LC is evaluated based on a statistical mechanical approach, i.e., a mean-field analysis, similar to that reported in references [13, 14], and the criterion for the determination of σ is obtained from the evaluation result. The proposed weight-initialization method is identical to Xavier initialization [18] in a specific case. In section 4, the proposed weight-initialization method is applied to RBM learning experiments, and the obtained numerical results support the validity of the proposed weight-initialization method. Section 5 summarizes this study and discusses the future scope.

2 Restricted Boltzmann Machine

Consider an RBM in which the visible and hidden layers consist of n visible and m hidden variables, $\mathbf{v} := \{v_i \mid i \in V := \{1, 2, \dots, n\}\}$ and $\mathbf{h} := \{h_j \mid j \in H := \{1, 2, \dots, m\}\}$, respectively. The visible and hidden variables are supposed to be binary discrete: $v_i \in \mathcal{X}_v := \{-1, 1\}$ and $h_j \in \mathcal{X}_h$ where $\mathcal{X}_h = \mathcal{B} := \{0, 1\}$ or $\mathcal{X}_h = \mathcal{I} := \{-1, 1\}$, i.e., this RBM is a Bernoulli–Bernoulli RBM. The RBM is expressed as

$$P(\mathbf{v}, \mathbf{h} \mid \theta) := \frac{1}{Z(\theta)} \exp \left(\sum_{i \in V} b_i v_i + \sum_{j \in H} c_j h_j + \sum_{i \in V} \sum_{j \in H} w_{i,j} v_i h_j \right), \quad (1)$$

where $Z(\theta)$ represents the partition function defined as

$$Z(\theta) := \sum_{\mathbf{v}} \sum_{\mathbf{h}} \exp \left(\sum_{i \in V} b_i v_i + \sum_{j \in H} c_j h_j + \sum_{i \in V} \sum_{j \in H} w_{i,j} v_i h_j \right),$$

where $\sum_{\mathbf{v}}$ and $\sum_{\mathbf{h}}$ denote multiple summations over all possible configurations of assigned variables, e.g., $\sum_{\mathbf{v}} = \sum_{v_1 \in \mathcal{X}_v} \sum_{v_2 \in \mathcal{X}_v} \cdots \sum_{v_n \in \mathcal{X}_v}$. Here, $\mathbf{b} := \{b_i \mid i \in V\}$ and $\mathbf{c} = \{c_j \mid j \in H\}$ are the biases for visible and hidden variables, respectively, and $\mathbf{w} := \{w_{i,j} \mid i \in V, j \in H\}$ are the weights between the visible and hidden layers. These learning parameters are collectively denoted by θ . For a give dataset consisting of N data points, $D := \{\mathbf{v}^{(\mu)} \in \mathcal{X}_v^n \mid \mu = 1, 2, \dots, N\}$, the log likelihood is defined as

$$L(\theta) := \frac{1}{N} \sum_{\mu=1}^N \ln P(\mathbf{v}^{(\mu)} \mid \theta), \quad (2)$$

where $P(\mathbf{v} \mid \theta)$ is the marginal distribution of RBM: $P(\mathbf{v} \mid \theta) = \sum_{\mathbf{h}} P(\mathbf{v}, \mathbf{h} \mid \theta)$. The RBM learning is archived by the maximization of the log likelihood with respect to the learning parameters. Usually,

the maximization is performed based on a gradient-based method. However, the gradients of the log likelihood includes the expectations of the RBM, whose evaluation is computationally infeasible when the size of the RBM is large. Practical approximate learning methods have been proposed, e.g., contrastive divergence (CD) [2], parallel tempering [20], and spatial Monte Carlo integration [21].

The learning parameters in the RBM, θ , are initialized at the beginning of the RBM learning. In this study, we consider an initialization in which the visible and hidden biases are initialized to constant values, $b_i = b$ and $c_j = c$, and the weights are initialized by small random values generated from a distribution $P_{\text{ini}}(\mathbf{w})$. The initial value of the visible biases, b , is fixed to zero, and that of the hidden biases, c , is set to zero when $\mathcal{X}_h = \mathcal{I}$, and to zero or a negative value when $\mathcal{X}_h = \mathcal{B}$. The negative value initialization encourages sparse representations of the hidden layer [22]. Therefore, the initial RBM is expressed as

$$P(\mathbf{v}, \mathbf{h} \mid \theta_{\text{ini}}) \propto \exp \left(b \sum_{i \in V} v_i + c \sum_{j \in H} h_j + \sum_{i \in V} \sum_{j \in H} w_{i,j} v_i h_j \right), \quad (3)$$

where \mathbf{w} are the initial weights drawn from $P_{\text{ini}}(\mathbf{w})$. In the initial RBM, b should vanish because it is fixed to zero in our initialization. However, we leave b in this expression for the convenience of the subsequent analysis. In this study, \mathbf{w} are independently drawn from a Gaussian distribution with zero mean and standard deviation $\sigma := \beta / \sqrt{n + m}$:

$$P_{\text{ini}}(\mathbf{w}) = P_{\text{ini}}(\mathbf{w} \mid \beta) = \prod_{i \in V} \prod_{j \in H} \frac{1}{\sqrt{2\pi\beta^2}} \exp \left(-\frac{w_{i,j}^2}{2\beta^2} \right),$$

where β is a nonnegative value. When $\mathcal{X}_h = \mathcal{I}$, the initial RBM corresponds to a bipartite Sherrington–Kirkpatrick (SK) model [15].

This study aims to find the value of β that can increase the learning efficiency. The learning efficiency mentioned here is considered as the growth rate of the training likelihood. Our hypothesis is that the distribution which has a large LC between the visible and hidden layers is more efficient. The information of one layer is more easily transferred to the other layer when the LC is larger. The smooth transfer of information in the initial state increases the learning efficiency at least in the early stage of learning. In the initial RBM presented in equation (3), we consider a statistical average of the sum-of-covariances defined by

$$\chi(\beta) \propto \sum_{i \in V} \sum_{j \in H} \int_{-\infty}^{+\infty} d\mathbf{w} P_{\text{ini}}(\mathbf{w} \mid \beta) \left(\mathbb{E}_{\text{ini}}[v_i h_j] - \mathbb{E}_{\text{ini}}[v_i] \mathbb{E}_{\text{ini}}[h_j] \right), \quad (4)$$

as the LC, where $\mathbb{E}_{\text{ini}}[\dots]$ represents the expectation on the initial RBM. The LC in equation (4) includes the covariances between the visible and hidden variables. In our hypothesis, the β value that maximizes $|\chi(\beta)|$,

$$\beta_{\text{max}} := \arg \max_{\beta} |\chi(\beta)|, \quad (5)$$

would be the most efficient. Therefore, the proposed initialization is summarized as follows: the biases \mathbf{b} and \mathbf{c} are initialized to constant values, i.e., $b_i = 0$ and $c_j = 0$ when $\mathcal{X}_h = \mathcal{I}$ and $b_i = 0$ and $c_j = c$, where $c \leq 0$, when $\mathcal{X}_h = \mathcal{B}$; further, the weights \mathbf{w} are initialized by small random values independently drawn from a Gaussian distribution with zero mean and standard deviation $\beta_{\text{max}} / \sqrt{n + m}$. Note that when $c = 0$ and $\beta_{\text{max}} = \sqrt{2}$, the proposed weight initialization is identical to that of the Xavier (Glorot) initialization [18].

An interpretation of the LC from a statistical mechanical point of view is as follows. Here, we define a (statistical-averaged) free energy as

$$f(\beta) := -\frac{1}{n+m} \int_{-\infty}^{+\infty} d\mathbf{w} P_{\text{ini}}(\mathbf{w} | \beta) \ln Z(\theta_{\text{ini}}). \quad (6)$$

The LC can be obtained from the free energy as

$$\chi(\beta) \propto -\frac{\partial^2 f(\beta)}{\partial b \partial c}. \quad (7)$$

The evaluation of the free energy is therefore essential. The free-energy evaluation will be discussed in the next section. The right-hand side of equation (7) is rewritten as

$$-\frac{\partial^2 f(\beta)}{\partial b \partial c} = \frac{\partial}{\partial b} \left(\sum_{j \in H} \int_{-\infty}^{+\infty} d\mathbf{w} P_{\text{ini}}(\mathbf{w} | \beta) \mathbb{E}_{\text{ini}}[h_j] \right).$$

This expression allows the LC to be viewed as the response of the hidden layer (i.e., the expectations of hidden variables) to the stimulus to the visible layer (i.e., the change of visible bias). The LC can be understood as a magnetic susceptibility.

3 Statistical Mechanical Analysis

The free energy and layer-correlation in equations (6) and (4), respectively, are evaluated based on the replica method [23, 24] which has been developed in the field of statistical mechanics. For the evaluation, we assume that the sizes of both layers, n and m , are sufficiently large; the ratio of both, $\alpha = m/n$, is fixed; and the magnitude of α is $O(1)$ for the layer sizes. The free energy in equation (6) is rewritten as

$$f(\beta) = -\frac{1}{n+m} \lim_{x \rightarrow 0} \frac{\Phi_x(\beta) - 1}{x}, \quad (8)$$

where

$$\Phi_x(\beta) := \int_{-\infty}^{+\infty} d\mathbf{w} P_{\text{ini}}(\mathbf{w} | \beta) Z(\theta_{\text{ini}})^x. \quad (9)$$

In the replica method, $\Phi_x(\beta)$ is evaluated in which x is limited to natural numbers. Subsequently, x is extended to real numbers via analytic continuation, and the limit of $x \rightarrow 0$ is considered for the evaluation result to obtain the free energy according to equation (8) (this is the so-called *replica trick*).

3.1 Free energy evaluation based on replica method

Using the replica method with the replica-symmetric (RS) assumption [23, 24], for $n, m \rightarrow +\infty$, equation (9) can be expressed as

$$\begin{aligned} \Phi_x(\beta) = \varepsilon(x) \exp xn \left[-\frac{\alpha\beta^2}{2(1+\alpha)} q_v q_h + \frac{1}{2} \hat{q}_v (q_v - 1) + \frac{\alpha}{2} \hat{q}_h q_h + \int_{-\infty}^{+\infty} Dz \ln \sum_{v \in \mathcal{X}_v} \exp(-E_v(v, z)) \right. \\ \left. + \alpha \int_{-\infty}^{+\infty} Dz \ln \sum_{h \in \mathcal{X}_h} \exp(-E_h(h, z)) + O(x) \right], \end{aligned} \quad (10)$$

where $\varepsilon(x) := (2\pi)^{-x(x-1)}$. Here,

$$\begin{aligned} E_v(v, z) &:= -(b + z\sqrt{\hat{q}_v})v, \\ E_h(h, z) &:= -(c + z\sqrt{\hat{q}_h})h - \frac{1}{2}\left(\frac{\beta^2}{1+\alpha} - \hat{q}_h\right)h^2 \end{aligned}$$

are the effective energies, and

$$\int_{-\infty}^{+\infty} Dz := \frac{1}{\sqrt{2\pi}} \int_{-\infty}^{+\infty} dz \exp\left(-\frac{z^2}{2}\right)$$

represents the standard Gauss measure. In this expression, q_v and q_h are regarded as the order parameters, and \hat{q}_v and \hat{q}_h are the auxiliary parameters. The order and auxiliary parameters are the solution to the saddle point equations, i.e., they are the solution to the extremum condition of the exponent of equation (10). In equation (10), x is assumed to be a real number that is negligible small. The derivation of equation (10) is described in Appendix A.

From equations (8) and (10), we obtain the free energy expression as

$$\begin{aligned} f(\beta) &\approx \frac{\alpha\beta^2}{2(1+\alpha)^2}q_vq_h - \frac{1}{2(1+\alpha)}\hat{q}_v(q_v - 1) - \frac{\alpha}{2(1+\alpha)}\hat{q}_hq_h - \frac{1}{1+\alpha} \int_{-\infty}^{+\infty} Dz \ln \sum_{v \in \mathcal{X}_v} \exp(-E_v(v, z)) \\ &\quad - \frac{\alpha}{1+\alpha} \int_{-\infty}^{+\infty} Dz \ln \sum_{h \in \mathcal{X}_h} \exp(-E_h(h, z)). \end{aligned} \quad (11)$$

In equation (11), q_v , q_h , \hat{q}_v , and \hat{q}_h are the solution to the saddle point equations, i.e., the extremum condition of the free energy. From the extremum condition of the free energy, the following saddle point equations are obtained.

$$\begin{pmatrix} \hat{q}_v \\ \hat{q}_h \end{pmatrix} = \beta^2 \mathbf{T}_\alpha \begin{pmatrix} q_v \\ q_h \end{pmatrix}, \quad \text{where } \mathbf{T}_\alpha := \frac{1}{1+\alpha} \begin{pmatrix} 0 & \alpha \\ 1 & 0 \end{pmatrix}, \quad (12)$$

$$q_v = \int_{-\infty}^{+\infty} Dz \mathbb{E}_v[v | z]^2 = \int_{-\infty}^{+\infty} Dz \tanh^2(b + z\sqrt{\hat{q}_v}), \quad (13)$$

and

$$q_h = \int_{-\infty}^{+\infty} Dz \mathbb{E}_h[h | z]^2 = \begin{cases} \int_{-\infty}^{+\infty} Dz \tanh^2(c + z\sqrt{\hat{q}_h}), & \mathcal{X}_h = \mathcal{I} \\ \int_{-\infty}^{+\infty} Dz \operatorname{sig}\left(c + \frac{\beta^2}{2(1+\alpha)} - \frac{\hat{q}_h}{2} + z\sqrt{\hat{q}_h}\right)^2, & \mathcal{X}_h = \mathcal{B} \end{cases}. \quad (14)$$

Here, $\operatorname{sig}(x) := 1/(1 + e^{-x})$ is the sigmoid function and

$$\begin{aligned} \mathbb{E}_v[\cdots | z] &:= \frac{\sum_{v \in \mathcal{X}_v} (\cdots) \exp(-E_v(v, z))}{\sum_{v \in \mathcal{X}_v} \exp(-E_v(v, z))}, \\ \mathbb{E}_h[\cdots | z] &:= \frac{\sum_{h \in \mathcal{X}_h} (\cdots) \exp(-E_h(h, z))}{\sum_{h \in \mathcal{X}_h} \exp(-E_h(h, z))}. \end{aligned}$$

A partial integration below was used in the derivations of equations (13) and (14). For function $f(z)$ that satisfies $\lim_{z \rightarrow \pm\infty} f(z) \exp(-z^2/2) = 0$, because $\partial \exp(-z^2/2)/\partial z = -z \exp(-z^2/2)$,

$$\int_{-\infty}^{+\infty} Dz z f(z) = \int_{-\infty}^{+\infty} Dz \frac{\partial f(z)}{\partial z}. \quad (15)$$

is obtained using the partial integration. When $\mathcal{X}_h = \mathcal{I}$, the expression of the free energy in equation (11) is essentially the same as the ones obtained in references [13, 14, 15]. The saddle point equations in equations (12), (13), and (14) can be numerically solved using a successive substitution or newton methods.

When $\mathcal{X}_h = \mathcal{I}$ and $b = c = 0$, the saddle point equations always have a trivial solution that is $q_v = q_h = \hat{q}_v = \hat{q}_h = 0$. It is known that there exists a specific critical point, $\beta = \beta_{\text{critical}}$, such that the saddle point equations have only the trivial solution when $\beta < \beta_{\text{critical}}$ (called the paramagnetic phase) and have not only the trivial solution but also a nontrivial positive solution when $\beta > \beta_{\text{critical}}$ (called the spin-glass phase). Such the critical point is called the *spin-glass transition point* (more properly, the paramagnetic and spin-glass phase transition point) [15]. When $\beta > \beta_{\text{critical}}$, the nonzero solution is selected. The spin-glass transition point is obtained as [13, 14]

$$\beta_{\text{critical}}^2 = \sqrt{\alpha} + \frac{1}{\sqrt{\alpha}}. \quad (16)$$

3.2 Layer-correlation evaluation

The LC in equation (4) is evaluated according to equation (7). In the following, q_v , q_h , \hat{q}_v , and \hat{q}_h represent the solution to the saddle point equations (12), (13), and (14). The derivatives of the negative of free energy in equation (11) with respect to b and c are

$$m_v := -\frac{\partial f(\beta)}{\partial b} = \frac{1}{1+\alpha} \int_{-\infty}^{+\infty} Dz \mathbb{E}_v[v | z], \quad (17)$$

$$m_h := -\frac{\partial f(\beta)}{\partial c} = \frac{\alpha}{1+\alpha} \int_{-\infty}^{+\infty} Dz \mathbb{E}_h[h | z], \quad (18)$$

respectively. From equation (7), the LC can be obtained by $\chi(\beta) \propto \partial m_h / \partial b$. We obtain the LC by evaluating susceptibility matrix $\chi_{\ell,k} := \partial m_\ell / \partial b_k$ where $\ell, k \in \{v, h\}$; here, $b_v = b$ and $b_h = c$.

For $\ell, k \in \{v, h\}$, the following equation is obtained.

$$\chi_{\ell,k} = \frac{\tau_\ell}{1+\alpha} \delta(\ell, k) \int_{-\infty}^{+\infty} Dz \{E_\ell^{(2)}(z) - E_\ell^{(1)}(z)^2\} - \frac{\tau_\ell}{1+\alpha} \hat{Q}_{\ell,k} \int_{-\infty}^{+\infty} Dz E_\ell^{(1)}(z) \{E_\ell^{(2)}(z) - E_\ell^{(1)}(z)^2\}, \quad (19)$$

where $\tau_\ell = \delta(v, \ell) + \alpha \delta(h, \ell)$,

$$E_\ell^{(m)}(z) := \begin{cases} \mathbb{E}_v[v^m | z], & \ell = v \\ \mathbb{E}_h[h^m | z], & \ell = h \end{cases}, \quad (20)$$

and matrix $\hat{Q}_{\ell,k}$ is defined by $\hat{Q}_{\ell,k} := \partial \hat{q}_\ell / \partial b_k$. Here, $\delta(\ell, k)$ represents the Kronecker delta function. Matrix $Q_{\ell,k} := \partial q_\ell / \partial b_k$ is obtained as

$$Q_{\ell,k} = 2\delta(\ell, k) \int_{-\infty}^{+\infty} Dz E_\ell^{(1)}(z) \{E_\ell^{(2)}(z) - E_\ell^{(1)}(z)^2\}$$

$$+ \hat{Q}_{\ell,k} \int_{-\infty}^{+\infty} Dz \{E_{\ell}^{(2)}(z)^2 - 4E_{\ell}^{(2)}(z)E_{\ell}^{(1)}(z)^2 + 3E_{\ell}^{(1)}(z)^4\}. \quad (21)$$

The partial integration in equation (15) was used to derive equations (19) and (21). From equations (19), and (21), the matrix expression of the susceptibility matrix can be obtained as

$$\chi = \hat{T}_{\alpha} \mathbf{V} - \hat{T}_{\alpha} \mathbf{U} \hat{\mathbf{Q}}, \quad (22)$$

$$\mathbf{Q} = 2\mathbf{U} + \mathbf{W} \hat{\mathbf{Q}}, \quad (23)$$

where χ , \mathbf{Q} , $\hat{\mathbf{Q}}$, and \hat{T}_{α} are 2×2 matrices defined by

$$\chi := \begin{pmatrix} \chi_{v,v} & \chi_{v,h} \\ \chi_{h,v} & \chi_{h,h} \end{pmatrix}, \quad \mathbf{Q} := \begin{pmatrix} Q_{v,v} & Q_{v,h} \\ Q_{h,v} & Q_{h,h} \end{pmatrix}, \quad \hat{\mathbf{Q}} := \begin{pmatrix} \hat{Q}_{v,v} & \hat{Q}_{v,h} \\ \hat{Q}_{h,v} & \hat{Q}_{h,h} \end{pmatrix}, \quad \text{and} \quad \hat{T}_{\alpha} := \frac{1}{1+\alpha} \begin{pmatrix} 1 & 0 \\ 0 & \alpha \end{pmatrix},$$

respectively, and \mathbf{V} , \mathbf{U} , and \mathbf{W} are 2×2 diagonal matrices defined by

$$\mathbf{V} := \begin{pmatrix} V_v & 0 \\ 0 & V_h \end{pmatrix}, \quad \mathbf{U} := \begin{pmatrix} U_v & 0 \\ 0 & U_h \end{pmatrix}, \quad \text{and} \quad \mathbf{W} := \begin{pmatrix} W_v & 0 \\ 0 & W_h \end{pmatrix},$$

respectively, where the elements of these diagonal matrices are defined by

$$\begin{aligned} V_{\ell} &:= \int_{-\infty}^{+\infty} Dz \{E_{\ell}^{(2)}(z) - E_{\ell}^{(1)}(z)^2\}, \\ U_{\ell} &:= \int_{-\infty}^{+\infty} Dz E_{\ell}^{(1)}(z) \{E_{\ell}^{(2)}(z) - E_{\ell}^{(1)}(z)^2\}, \\ W_{\ell} &:= \int_{-\infty}^{+\infty} Dz \{E_{\ell}^{(2)}(z)^2 - 4E_{\ell}^{(2)}(z)E_{\ell}^{(1)}(z)^2 + 3E_{\ell}^{(1)}(z)^4\}, \end{aligned}$$

for $\ell \in \{v, h\}$. From equation (12),

$$\hat{\mathbf{Q}} = \beta^2 \mathbf{T}_{\alpha} \mathbf{Q}. \quad (24)$$

From equations (22), (23), and (24), we obtain the expression of the susceptibility matrix as

$$\chi = \hat{T}_{\alpha} \{ \mathbf{V} - 2\beta^2 \mathbf{U} \mathbf{T}_{\alpha} (\mathbf{I} - \beta^2 \mathbf{W} \mathbf{T}_{\alpha})^{-1} \mathbf{U} \}, \quad (25)$$

where \mathbf{I} represents a 2×2 identity matrix. The LC corresponds to the off-diagonal elements of the susceptibility matrix, i.e., $\chi(\beta) \propto \chi_{v,h}$. The susceptibility matrix is numerically obtained by substituting the solution to the saddle point equations (12), (13), and (14) to equation (25).

The objective is to find the value of β that maximizes the absolute value of the LC. Since $\chi(\beta) \propto \chi_{v,h}$, the desired value is obtained by

$$\beta_{\max} = \arg \max_{\beta} |\chi_{v,h}|. \quad (26)$$

The dependency of $|\chi_{v,h}|$ on β is demonstrated using numerical experiments. Figure 1 depicts the dependency of $|\chi_{v,h}|$ on β when $\mathcal{X}_h = \mathcal{B}$ for $\alpha = 0.5, 1, 2$ and $c = 0, -5$, in which $b = 0$ was fixed. Figure 2 depicts the dependency of $|\chi_{v,h}|$ on β when $\mathcal{X}_h = \mathcal{I}$ for $\alpha = 0.5, 1, 1.5$, in which $b = c = 0$ were fixed.

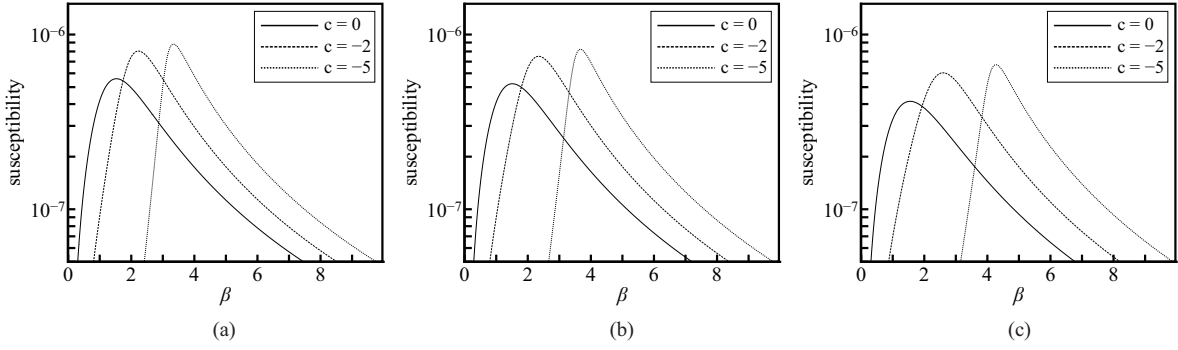


Figure 1: Dependency of $|\chi_{v,h}|$ on β when $\mathcal{X}_h = \mathcal{B}$: (a) $\alpha = 0.5$, (b) $\alpha = 1$, and (c) $\alpha = 2$.

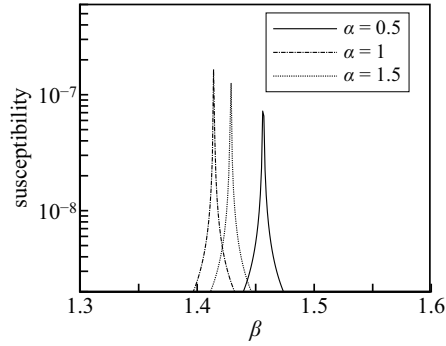


Figure 2: Dependency of $|\chi_{v,h}|$ on β when $\mathcal{X}_h = \mathcal{I}$.

Figures 1 and 2 show that $|\chi_{v,h}|$ has the unique maximum at the specific finite value of β . The values of β_{\max} for various α s and c s are listed in Appendix B ¹.

In the following, we consider the case where $\mathcal{X}_h = \mathcal{I}$ and $b = c = 0$. In this case, a singular behavior of the susceptibility is observed at $\beta = \beta_{\max}$ as shown in figure 2. Such a singular behavior can occur at transition points in many physical systems. In fact, in the original SK model [25] which has many physical features in common with the bipartite SK model, it is known that a cusp of the susceptibility appears at the spin-glass transition point. Moreover, the expression as equation (16) agrees with the numerical results listed in table 7 in Appendix B. Therefore, we can conclude

$$\beta_{\max}^2 = \beta_{\text{critical}}^2 = \sqrt{\alpha} + \frac{1}{\sqrt{\alpha}}. \quad (27)$$

In a physical interpretation, a model at the transition point is considered unstable which means that the model can easily change its physical state by a small perturbation. Therefore, setting the initial RBM at the transition point seems to be reasonable because such RBM can easily move by a small parameter update. It is noteworthy that from equation (27), $\beta_{\max}^2 = 2$ when $\alpha = 1$; thus, the proposed weight

¹In the experiments demonstrated here (and the experiments to obtain the results listed in table 7 in Appendix B), when $\mathcal{X}_h = \mathcal{I}$, the values of $|\chi_{v,h}|$ obtained when $b = c = 0$ were very small and can be buried in numerical errors (e.g., error of numerical integration). For example, in this case, $\chi = \mathbf{0}$ when $\beta < \beta_{\text{critical}}$ because $q_v = q_h = \hat{q}_v = \hat{q}_h = 0$. Therefore, we used a very small positive value $\varepsilon \ll 1$ instead of zero, i.e., $b = c = 0$ means $b = c = \varepsilon$, to emphasize the behavior around $\beta = \beta_{\max}$. Whereas, the other cases, i.e., the cases with $\mathcal{X}_h = \mathcal{B}$, true zero was used.

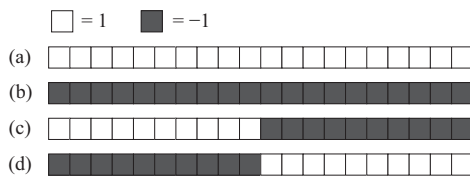


Figure 3: Four base-patterns with $n = 20$ elements: (a) all are 1, (b) all are -1 , (c) the first 10 elements are 1 and the others are -1 , and (d) the reverse of (c).

initialization is identical to that of the Xavier initialization [18] when $\mathcal{X}_h = \mathcal{I}$, $b = c = 0$, and $\alpha = 1$ (i.e., when the initial RBM is identical to the Korenblit–Shender model with zero bias [26]).

4 Numerical Experiment

The efficiency of the proposed weight initialization is demonstrated using learning experiments based on a toy and MNIST datasets. The efficiency of learning is considered as the growth rate of the log-likelihood in equation (2).

4.1 Toy dataset

Table 1: Training log-likelihoods versus training epoch when $\mathcal{X}_h = \mathcal{I}$ and $c = 0$.

		$\alpha = 0.5$			$\alpha = 1$			$\alpha = 1.5$		
		epoch			epoch			epoch		
		0	100	200	0	100	200	0	100	200
β	$\beta_{\max}/4$	-13.88	-9.75	-9.64	-13.88	-9.73	-9.51	-13.88	-9.71	-9.44
	$\beta_{\max}/2$	-14.08	-9.73	-9.62	-14.09	-9.67	-9.45	-14.07	-9.63	-9.34
	β_{\max}	-15.76	-9.73	-9.61	-16.07	-9.62	-9.42	-16.31	-9.54	-9.27
	$2\beta_{\max}$	-22.99	-10.06	-9.72	-25.69	-9.93	-9.53	-26.88	-9.75	-9.35
	$4\beta_{\max}$	-44.25	-13.89	-11.28	-49.03	-13.24	-10.95	-52.97	-12.81	-10.57

Table 2: Training log-likelihoods versus training epoch when $\mathcal{X}_h = \mathcal{B}$ and $c = 0$.

		$\alpha = 0.5$			$\alpha = 1$			$\alpha = 1.5$		
		epoch			epoch			epoch		
		0	100	200	0	100	200	0	100	200
β	$\beta_{\max}/4$	-14.00	-9.82	-9.76	-14.05	-9.85	-9.75	-14.08	-9.87	-9.74
	$\beta_{\max}/2$	-14.42	-9.82	-9.76	-14.61	-9.84	-9.73	-14.78	-9.84	-9.71
	β_{\max}	-16.37	-9.83	-9.76	-16.95	-9.82	-9.71	-17.50	-9.82	-9.69
	$2\beta_{\max}$	-24.12	-10.07	-9.82	-26.35	-9.96	-9.77	-28.14	-9.94	-9.72
	$4\beta_{\max}$	-42.93	-12.79	-10.68	-49.25	-11.81	-10.57	-52.51	-11.46	-10.38

The learning results using a toy dataset with $n = 20$ and $N = 400$ are presented in this section. The toy dataset was obtained by the following procedure. First, the four base-patterns illustrated in figure 3 were prepared. Next, from each pattern, 100 data points were generated with 15% randomly flipping. A

Table 3: Training log-likelihoods versus training epoch when $\mathcal{X}_h = \mathcal{B}$ and $c = -5$.

		$\alpha = 0.5$			$\alpha = 1$			$\alpha = 1.5$		
		epoch			epoch			epoch		
		0	100	200	0	100	200	0	100	200
β	$\beta_{\max}/4$	-13.86	-10.00	-9.88	-13.86	-9.94	-9.78	-13.86	-9.95	-9.76
	$\beta_{\max}/2$	-13.87	-9.97	-9.81	-13.87	-9.87	-9.68	-13.87	-9.86	-9.58
	β_{\max}	-15.04	-10.05	-9.79	-15.38	-9.85	-9.60	-15.60	-9.77	-9.43
	$2\beta_{\max}$	-32.28	-12.72	-10.65	-39.22	-12.13	-10.65	-43.31	-12.13	-10.65
	$4\beta_{\max}$	-76.55	-29.60	-18.70	-102.61	-32.05	-19.85	-110.25	-30.75	-20.30

total of $N = 400$ data points were obtained using this procedure. This toy dataset is similar to that used in reference [20].

For the toy dataset, the RBMs with $n = 20$ and $m = 10, 20, 30$ (i.e., $\alpha = 0.5, 1, 1.5$) were used. The log likelihood and its gradients can be computed exactly because the sizes of the RBMs are not large. Based on the exact gradients, the maximization of the log likelihood was conducted using the Adam optimizer [27] with a learning rate of 0.01, in which batch learning was employed. The values of β_{\max} for each experiments were the corresponding values listed in Appendix B. For comparison, the experiments when $\beta = \beta_{\max}/4, \beta_{\max}/2, 2\beta_{\max}$, and $4\beta_{\max}$ were also conducted. The results of experiments are listed in Tables 1–3. The listed values are the average over 100 experiments. The log likelihoods rise with increasing the training epoch. After 200 epochs, the result of $\beta = \beta_{\max}$ is the best in terms of the log likelihood in all experiments.

4.2 MNIST dataset

Table 4: Training log-likelihoods versus training epoch when $\mathcal{X}_h = \mathcal{I}$ and $c = 0$. $\beta_{\max} \approx 1.432$.

		epoch		
		25	50	75
β	$\beta_{\max}/4$	-128.5	-113.1	-106.5
	$\beta_{\max}/2$	-115.9	-101.6	-97.0
	β_{\max}	-106.1	-94.8	-90.1
	$2\beta_{\max}$	-111.8	-98.5	-92.1
	$4\beta_{\max}$	-148.2	-132.2	-123.1

The learning results using a MNIST dataset are shown in this section. MNIST is a dataset of hand-written digit images, i.e., $0, 1, \dots, 9$, in which each input image is a 28×28 grayscale digit image. In the experiments in this section, we used $N = 3000$ data points randomly selected from the MNIST dataset, and each input image was binarized to \mathcal{I} using the Otsu binarization method [28].

RBMs with $n = 784$ and $m = 500$ (i.e., $\alpha \approx 0.64$) were used for the dataset. The sizes of the RBMs are large, and therefore, an approximation method has to be employed in the learning and log likelihood evaluation. The 10-steps CD (i.e., CD_{10}) method was used in the learning, and the marginalized annealed importance sampling [29] was used in the log likelihood evaluation. The maximization of the log likelihood was conducted using the Adam optimizer with a learning rate of 0.001, in which a mini-batch learning with mini-batch size of 100 was employed. For comparison, the experiments when $\beta = \beta_{\max}/4, \beta_{\max}/2, 2\beta_{\max}$, and β_{\max} were also conducted. The results of the experiments are listed in Tables 4 and 5. The value

Table 5: Training log-likelihoods versus training epoch when $\mathcal{X}_h = \{0, 1\}$. $\beta_{\max} \approx 1.516, 2.463, 3.428$ for $c = 0, -2.5,$ and $-5,$ respectively.

		$c = 0$			$c = -2.5$			$c = -5$		
		epoch			epoch			epoch		
		25	50	75	25	50	75	25	50	75
β	$\beta_{\max}/4$	-147.3	-120.8	-108.9	-124.7	-105.0	-95.4	-117.4	-99.9	-91.6
	$\beta_{\max}/2$	-143.8	-120.2	-108.5	-120.1	-102.1	-93.9	-108.9	-95.0	-87.2
	β_{\max}	-121.1	-104.5	-95.5	-105.7	-92.9	-86.2	-102.9	-90.3	-84.1
	$2\beta_{\max}$	-112.4	-97.7	-90.2	-110.2	-95.5	-87.8	-118.8	-102.0	-94.2
	$4\beta_{\max}$	-123.2	-105.4	-96.3	-182.7	-141.5	-123.3	-352.5	-343.5	-351.0

of β_{\max} for each experiment was obtained using equation (26). The listed values are the average over 30 experiments. The result of $\beta = \beta_{\max}$ is the best in terms of the log likelihood, except in the case of $\mathcal{X}_h = \mathcal{B}$ and $c = 0$ wherein the result of $\beta = \beta_{\max}$ is the second best.

In the experiments in sections 4.1 and 4.2, the proposed weight initialization exhibits the best or at least the second best performance in the perspective of the growth rate of the log-likelihood. These results supports our hypothesis discussed in section 2.

5 Summary and Future Studies

Based on the statistical mechanical approach, we propose an appropriate standard deviation, $\sigma = \beta/\sqrt{n+m}$, of the Gaussian distribution for the random weight-initialization of Bernoulli–Bernoulli RBMs in which the sample space of the visible variables is $\mathcal{X}_v = \mathcal{I}$ and that of the hidden variables is $\mathcal{X}_h = \mathcal{B}$ or $\mathcal{X}_h = \mathcal{I}$. In the proposed initialization, the biases of the visible layer are fixed to zero and those of the hidden layer are fixed to a constant $c \leq 0$. The appropriate β value, i.e., β_{\max} , is defined as the value that maximizes the absolute value of the LC between the visible and hidden layers. This criteria is based on our hypothesis discussed in section 2. The numerical results presented in section 4 support the validity of the proposed initialization. The β_{\max} value depends on only three components: the size ratio between visible and hidden layers $\alpha = m/n$, value of c , and \mathcal{X}_h . The examples of the β_{\max} value are listed in Appendix B.

Three remaining issues that should be addressed in future studies are as follows. First, the proposed initialization method dose not cover a Gaussian–Bernoulli RBM (GBRBM) that has a continuous visible layer [4, 30, 31, 32] and its variant model [33]. GBRBMs can treat continuous data, and therefore, they are more important for practical applications. To obtain an appropriate dataset-free initialization for the GBRBMs needs to be extended to the presented framework. An initialization method for RBMs with binary visible and continuous hidden layers was proposed based on the concept of the Hopfield neural network [34]. This work is different from ours because our objective model is an RBM with a continuous visible layer; however, the results obtained from this work can be a good reference of our future studies. Second, the explicit expression of β_{\max} as a function of α , c , and \mathcal{X}_h is unknown except for the case of $b = c = 0$ and $\mathcal{X}_h = \mathcal{I}$. Figures 1 and 2 indicate that $|\chi(\beta)|$ has a unique maximum at the specific β , and therefore, β_{\max} can be obtained numerically using a line search method. This numerical search is not computationally expensive (it often finishes within a few seconds in a Python implementation); however, the mathematical expression of β_{\max} is helpful for both practical and theoretical perspectives. Third, the proposed initialization is identical to Xavier initialization [18] when $\mathcal{X}_h = \mathcal{I}$, $b = c = 0$, and $\alpha = 1$. This

similarity would suggest some relationship between the concept of Xavier initialization (i.e., conservation of signal variances in forward and backward propagations) and our hypothesis. A deeper consideration for the relationship could gain an alternative insight into our hypothesis, increasing the reasonability of our hypothesis.

Acknowledgment

This work was partially supported by JSPS KAKENHI (Grant No. 21K11778). We would like to thank K. Koyama for the variable discussions.

A Replica Analysis

For a natural number x , performing the Gaussian integral in equation (9) yields

$$\Phi_x(\beta) = \sum_{\mathbf{v}_{\text{all}}} \sum_{\mathbf{h}_{\text{all}}} \exp \left\{ b \sum_{s=1}^x \sum_{i \in V} v_{i,s} + c \sum_{s=1}^x \sum_{j \in H} h_{j,s} + \frac{\beta^2}{2(n+m)} \sum_{i \in V} \sum_{j \in H} \left(\sum_{s=1}^x v_{i,s} h_{j,s} \right)^2 \right\},$$

where $s = 1, 2, \dots, x$ is the replica index, and $\mathbf{v}_{\text{all}} := \{v_{i,s} \in \{-1, +1\} \mid i \in V; s = 1, 2, \dots, x\}$ and $\mathbf{h}_{\text{all}} := \{h_{j,s} \in \mathcal{X}_H \mid j \in H; s = 1, 2, \dots, x\}$ are the visible and hidden variables in the x -replicated system. Because $v_{i,a} \in \{-1, +1\}$,

$$\begin{aligned} \Phi_x(\beta) = \sum_{\mathbf{v}_{\text{all}}} \sum_{\mathbf{h}_{\text{all}}} \exp \left\{ b \sum_{s=1}^x \sum_{i \in V} v_{i,s} + c \sum_{s=1}^x \sum_{j \in H} h_{j,s} + \frac{\beta^2}{n+m} \sum_{s < t}^x \left(\sum_{i \in V} v_{i,s} v_{i,t} \right) \left(\sum_{j \in H} h_{j,s} h_{j,t} \right) \right. \\ \left. + \frac{n\beta^2}{2(n+m)} \sum_{s=1}^x \sum_{j \in H} h_{j,s}^2 \right\}, \end{aligned} \quad (28)$$

where $\sum_{s < t}^x$ denotes the sum over all distinct pairs of replicas, i.e., $\sum_{s < t}^x = \sum_{s=1}^x \sum_{t=s+1}^x$. Using the Dirac delta function, equation (28) is rewritten as

$$\begin{aligned} \Phi_x(\beta) = \int_{-\infty}^{+\infty} d\mathbf{q}^{(\text{v})} \int_{-\infty}^{+\infty} d\mathbf{q}^{(\text{h})} \sum_{\mathbf{v}_{\text{all}}} \sum_{\mathbf{h}_{\text{all}}} \exp \left\{ b \sum_{s=1}^x \sum_{i \in V} v_{i,s} + c \sum_{s=1}^x \sum_{j \in H} h_{j,s} + \frac{nm\beta^2}{n+m} \sum_{s < t}^x q_{s,t}^{(\text{v})} q_{s,t}^{(\text{h})} \right. \\ \left. + \frac{n\beta^2}{2(n+m)} \sum_{s=1}^x \sum_{j \in H} h_{j,s}^2 \right\} \left[\prod_{s < t}^x \delta \left(\sum_{i \in V} v_{i,s} v_{i,t} - n q_{s,t}^{(\text{v})} \right) \delta \left(\sum_{j \in H} h_{j,s} h_{j,t} - m q_{s,t}^{(\text{h})} \right) \right], \end{aligned}$$

where $\mathbf{q}^{(\text{v})} := \{q_{s,t}^{(\text{v})} \mid s < t; s, t = 1, 2, \dots, x\}$ and $\mathbf{q}^{(\text{h})} := \{q_{s,t}^{(\text{h})} \mid s < t; s, t = 1, 2, \dots, x\}$ are called *spin-glass order parameters* in statistical mechanics. Applying the Fourier integral expression of Dirac delta function,

$$\delta(x) = \frac{1}{2\pi} \int_{-\infty}^{+\infty} d\hat{x} \exp(i\hat{x}x),$$

where i is the imaginary number and \hat{x} is the auxiliary parameter, leads to

$$\Phi_x(\beta) = \varepsilon(x) \int_{-\infty}^{+\infty} d\mathbf{q}^{(\text{v})} \int_{-\infty}^{+\infty} d\mathbf{q}^{(\text{h})} \int_{-\infty}^{+\infty} d\hat{\mathbf{q}}^{(\text{v})} \int_{-\infty}^{+\infty} d\hat{\mathbf{q}}^{(\text{h})} \sum_{\mathbf{v}_{\text{all}}} \sum_{\mathbf{h}_{\text{all}}} \exp \left\{ b \sum_{s=1}^x \sum_{i \in V} v_{i,s} \right.$$

$$\begin{aligned}
& + c \sum_{s=1}^x \sum_{j \in H} h_{j,s} + \frac{nm\beta^2}{n+m} \sum_{s<t}^x q_{s,t}^{(v)} q_{s,t}^{(h)} + \frac{n\beta^2}{2(n+m)} \sum_{s=1}^x \sum_{j \in H} h_{j,s}^2 + i \sum_{s<t}^x \hat{q}_{s,t}^{(v)} \left(\sum_{i \in V} v_{i,s} v_{i,t} - n q_{s,t}^{(v)} \right) \\
& + i \sum_{s<t}^x \hat{q}_{s,t}^{(h)} \left(\sum_{j \in H} h_{j,s} h_{j,t} - m q_{s,t}^{(h)} \right) \},
\end{aligned}$$

where $\varepsilon(x) = (2\pi)^{-x(x-1)}$, and $\hat{\mathbf{q}}^{(v)}$ and $\hat{\mathbf{q}}^{(h)}$ are the auxiliary parameters of the Fourier integral expression. This is rewritten as

$$\begin{aligned}
\Phi_x(\beta) &= \varepsilon(x) \int_{-\infty}^{+\infty} d\mathbf{q}^{(v)} \int_{-\infty}^{+\infty} d\mathbf{q}^{(h)} \int_{-\infty}^{+\infty} d\hat{\mathbf{q}}^{(v)} \int_{-\infty}^{+\infty} d\hat{\mathbf{q}}^{(h)} \exp n \left\{ \frac{\alpha\beta^2}{1+\alpha} \sum_{s<t}^x q_{s,t}^{(v)} q_{s,t}^{(h)} \right. \\
& - i \sum_{s<t}^x \hat{q}_{s,t}^{(v)} q_{s,t}^{(v)} - \alpha i \sum_{s<t}^x \hat{q}_{s,t}^{(h)} q_{s,t}^{(h)} + \ln \sum_{\mathbf{v}^*} \exp \left(b \sum_{s=1}^x v_s^* + i \sum_{s<t}^x \hat{q}_{s,t}^{(v)} v_s^* v_t^* \right) \\
& \left. + \alpha \ln \sum_{\mathbf{h}^*} \exp \left(c \sum_{s=1}^x h_s^* + \frac{\beta^2}{2(1+\alpha)} \sum_{s=1}^x (h_s^*)^2 + i \sum_{s<t}^x \hat{q}_{s,t}^{(h)} h_s^* h_t^* \right) \right\}, \tag{29}
\end{aligned}$$

where $\mathbf{v}^* := \{v_s^* \in \{-1, +1\} \mid s = 1, 2, \dots, x\}$ and $\mathbf{h}^* := \{h_s^* \in \mathcal{X}_h \mid s = 1, 2, \dots, x\}$. In the limit of $n \rightarrow +\infty$, the multiple integration in equation (29) can be evaluated by the saddle point method (or the method of steepest descent). The saddle point method leads to

$$\begin{aligned}
\Phi_x(\beta) &= \varepsilon(x) \exp n \left\{ \frac{\alpha\beta^2}{1+\alpha} \sum_{s<t}^x q_{s,t}^{(v)} q_{s,t}^{(h)} - \sum_{s<t}^x \hat{q}_{s,t}^{(v)} q_{s,t}^{(v)} - \alpha \sum_{s<t}^x \hat{q}_{s,t}^{(h)} q_{s,t}^{(h)} + \ln \sum_{\mathbf{v}^*} \exp \left(b \sum_{s=1}^x v_s^* + \sum_{s<t}^x \hat{q}_{s,t}^{(v)} v_s^* v_t^* \right) \right. \\
& \left. + \alpha \ln \sum_{\mathbf{h}^*} \exp \left(c \sum_{s=1}^x h_s^* + \frac{\beta^2}{2(1+\alpha)} \sum_{s=1}^x (h_s^*)^2 + \sum_{s<t}^x \hat{q}_{s,t}^{(h)} h_s^* h_t^* \right) \right\}, \tag{30}
\end{aligned}$$

where $\mathbf{q}^{(v)}$, $\mathbf{q}^{(h)}$, $\hat{\mathbf{q}}^{(v)}$, and $\hat{\mathbf{q}}^{(h)}$ represent the saddle point which are the solution to the saddle point equations. The saddle point equations are obtained from the extremum condition of the exponent in equation (30). In equation (30), the reparameterizations, $i\hat{q}_{s,t}^{(v)} \rightarrow \hat{q}_{s,t}^{(v)}$ and $i\hat{q}_{s,t}^{(h)} \rightarrow \hat{q}_{s,t}^{(h)}$, were used without loss of the generality.

To proceed the analysis, we employ the RS assumption [23, 24] that the order and auxiliary parameters do not depend on their index in the saddle point, i.e., $q_{s,t}^{(v)} = q_v$, $q_{s,t}^{(h)} = q_h$, $\hat{q}_{s,t}^{(v)} = \hat{q}_v$, and $\hat{q}_{s,t}^{(h)} = \hat{q}_h$ hold in the saddle point. With this assumption, $\Phi_x(b, c, \beta)$ in equation (30) is expressed as

$$\begin{aligned}
\Phi_x(\beta) &= \varepsilon(x) \exp xn \left\{ \frac{(x-1)\alpha\beta^2}{2(1+\alpha)} q_v q_h - \frac{x-1}{2} \hat{q}_v q_v - \frac{(x-1)\alpha}{2} \hat{q}_h q_h + \frac{1}{x} \ln \sum_{\mathbf{v}^*} \exp \left(b \sum_{s=1}^x v_s^* + \hat{q}_v \sum_{s<t}^x v_s^* v_t^* \right) \right. \\
& \left. + \frac{\alpha}{x} \ln \sum_{\mathbf{h}^*} \exp \left(c \sum_{s=1}^x h_s^* + \frac{\beta^2}{2(1+\alpha)} \sum_{s=1}^x (h_s^*)^2 + \hat{q}_h \sum_{s<t}^x h_s^* h_t^* \right) \right\} \\
& = \varepsilon(x) \exp xn \left[\frac{(x-1)\alpha\beta^2}{2(1+\alpha)} q_v q_h + \frac{\hat{q}_v}{2} ((1-x)q_v - 1) - \frac{(x-1)\alpha}{2} \hat{q}_h q_h \right. \\
& \left. + \frac{1}{x} \ln \sum_{\mathbf{v}^*} \exp \left\{ b \sum_{s=1}^x v_s^* + \frac{1}{2} \left(\sqrt{\hat{q}_v} \sum_{s=1}^x v_s^* \right)^2 \right\} \right. \\
& \left. + \frac{\alpha}{x} \ln \sum_{\mathbf{h}^*} \exp \left\{ c \sum_{s=1}^x h_s^* + \frac{1}{2} \left(\frac{\beta^2}{1+\alpha} - \hat{q}_h \right) \sum_{s=1}^x (h_s^*)^2 + \frac{1}{2} \left(\sqrt{\hat{q}_h} \sum_{s=1}^x h_s^* \right)^2 \right\} \right]. \tag{31}
\end{aligned}$$

Applying the Hubbard–Stratonovich transformation,

$$\exp\left(\frac{\lambda}{2}a^2\right) = \sqrt{\frac{\lambda}{2\pi}} \int_{-\infty}^{+\infty} dz \exp\left(-\frac{\lambda}{2}z^2 + \lambda az\right),$$

to equation (31) provides equation (10). In equation (10), x is extended to a real number (i.e., replica trick).

B List of β_{\max}

Table 6 lists β_{\max} when $\mathcal{X}_h = \{0, 1\}$ for various values of α and c , in which b was fixed to zero. Table 7 lists β_{\max} when $\mathcal{X}_h = \{-1, 1\}$ for various values of α , in which b and c were fixed to zero. The values in these tables were obtained by numerically solving equation (26) using a simple line search method.

Table 6: List of β_{\max} for the various values of α and c when $\mathcal{X}_h = \{0, 1\}$.

		c						
		0	-1	-2	-3	-4	-5	-6
α	0.25	1.597	1.873	2.216	2.558	2.887	3.196	3.488
	0.5	1.529	1.840	2.227	2.618	2.989	3.338	3.666
	0.75	1.511	1.853	2.280	2.712	3.120	3.503	3.863
	1	1.510	1.879	2.344	2.812	3.255	3.669	4.058
	1.25	1.517	1.911	2.409	2.911	3.385	3.829	4.245
	1.5	1.527	1.944	2.473	3.007	3.512	3.982	4.424
	1.75	1.539	1.977	2.536	3.100	3.633	4.130	4.595
	2	1.551	2.009	2.596	3.190	3.749	4.271	4.759
	2.25	1.564	2.040	2.654	3.275	3.861	4.406	4.917
	2.5	1.576	2.070	2.710	3.358	3.968	4.536	5.069
	2.75	1.588	2.099	2.764	3.437	4.071	4.662	5.215
	3	1.600	2.127	2.815	3.514	4.171	4.783	5.356

Table 7: List of β_{\max} for the various values of α when $\mathcal{X}_h = \{-1, 1\}$. The listed values are in good agreement with the expression in equation (27).

α	0.5	1	1.5	2	2.5	3
β_{\max}	1.456	1.414	1.429	1.456	1.488	1.520

References

- [1] P. Smolensky. Information processing in dynamical systems: foundations of harmony theory. *Parallel distributed processing: Explorations in the microstructure of cognition*, 1:194–281, 1986.
- [2] G. E. Hinton. Training products of experts by minimizing contrastive divergence. *Neural Computation*, 8(14):1771–1800, 2002.

- [3] R. Salakhutdinov, A. Mnih, and G. Hinton. Restricted boltzmann machines for collaborative filtering. *Proceedings of the 24th International Conference on Machine Learning*, pages 791–798, 2007.
- [4] G. Hinton and R. Salakhutdinov. Reducing the dimensionality of data with neural networks. *Science*, 313(5786):504–507, 2006.
- [5] M. Yasuda and Z. Xiong. New learning algorithm of gaussian–bernoulli restricted boltzmann machine and its application in feature extraction. *In Proc. of the 2023 International Symposium on Nonlinear Theory and Its Applications*, pages 134–137, 2023.
- [6] H. Larochelle, M. Mandel, R. Pascanu, and Y. Bengio. Learning algorithms for the classification restricted boltzmann machine. *The Journal of Machine Learning Research*, 13(1):643–669, 2012.
- [7] Y. Yokoyama, T. Katsumata, and M. Yasuda. Restricted Boltzmann Machine with Multivalued Hidden Variables: a model suppressing over-fitting. *The Review of Socionetwork Strategies*, 13(2):253–266, 2019.
- [8] U. Fiore, F. Palmieri, A. Castiglione, and A. D. Santis. Network anomaly detection with the restricted boltzmann machine. *Neurocomputing*, 122(25):13–23, 2013.
- [9] K. Sekimoto, C. Takahashi, and M. Yasuda. Quasi-free energy evaluation of gaussian-bernoulli restricted boltzmann machine for anomaly detection. *Nonlinear Theory and Its Applications, IEICE*, 15(2):272–283, 2024.
- [10] G. E. Hinton, S. Osindero, and Y. W. Teh. A fast learning algorithm for deep belief net. *Neural Computation*, 18(7):1527–1554, 2006.
- [11] R. Salakhutdinov and G. E. Hinton. Deep boltzmann machines. *Proceedings of the 12th International Conference on Artificial Intelligence and Statistics (AISTATS 2009)*, pages 448–455, 2009.
- [12] Y. Kanno and M. Yasuda. Multi-layered Discriminative Restricted Boltzmann Machine with Untrained Probabilistic Layer. *In Proc. of the 25th International Conference on Pattern Recognition*, pages 7655–7660, 2021.
- [13] A. Barra, G. Genovese, and F. Guerra. Equilibrium statistical mechanics of bipartite spin systems. *Journal of Physics A: Mathematical and Theoretical*, 44(24):245002, 2011.
- [14] A Barra, G. Genovese, P. Sollich, and D. Tantari. Phase diagram of restricted boltzmann machines and generalized hopfield networks with arbitrary priors. *Phys. Rev. E*, 97(2):022310, 2017.
- [15] G. S. Hartnett, E. Parker, and E. Geist. Replica symmetry breaking in bipartite spin glasses and neural networks. *Phys. Rev. E*, 98(2):022116, 2018.
- [16] A. Decelle and C. Furtlehner. Restricted boltzmann machine: Recent advances and mean-field theory. *Chinese Physics B*, 30(4):040202, 2021.
- [17] Y. LeCun, L. Bottou, G. Orr, and K. Müller. Efficient backprop. *Neural Networks: Tricks of the Trade*, pages 9–48, 2012.
- [18] X. Glorot and Y. Bengio. Understanding the difficulty of training deep feedforward neural networks. *In Proc. of the 13th International Conference on Artificial Intelligence and Statistics*, 9:249–256, 2010.

- [19] K. He, X. Zhang, S. Ren, and J. Sun. Delving deep into rectifiers: Surpassing human-level performance on imagenet classification. *In Proc. of the 2015 IEEE International Conference on Computer Vision*, pages 1026–1034, 2015.
- [20] G. Desjardins, A. Courville, Y. Bengio, P. Vincent, and O. Delalleau. Parallel tempering for training of restricted boltzmann machines. *In Proc. of the 13th International Conference on Artificial Intelligence and Statistics*, pages 145–152, 2010.
- [21] K. Sekimoto and M. Yasuda. Effective learning algorithm for restricted boltzmann machines via spatial monte carlo integration. *Nonlinear Theory and its Applications, IEICE*, 14(2):228–241, 2023.
- [22] G. E. Hinton. A practical guide to training restricted boltzmann machines. *Neural Networks: Tricks of the Trade*, pages 599–619, 2012.
- [23] M. Mezard, G. Parisi, and M. Virasoro. *Spin Glass Theory and Beyond: An Introduction to the Replica Method and Its Applications*. Singapore: World Scientific, 1987.
- [24] H. Nishimori. *Statistical Physics of Spin Glass and Information Processing – Introduction–*. Oxford University Press, 2001.
- [25] D. Sherrington and S. Kirkpatrick. Solvable model of a spin-glass. *Physical Review Letters*, 35(26):1792–1796, 1975.
- [26] I. Y. Korenblit and E. F. Shender. Spin glass in an Ising two-sublattice magnet. *Soviet physics JETP*, 62(5):1030–1035, 1985.
- [27] D. P. Kingma and L. J. Ba. Adam: A method for stochastic optimization. *Proceedings of the 3rd International Conference on Learning Representations*, pages 1–13, 2015.
- [28] N. Otsu. A threshold selection method from gray-level histograms. *IEEE Transactions on Systems, Man, and Cybernetics*, 9(1):62–66, 1979.
- [29] M. Yasuda and C. Takahashi. Free energy evaluation using marginalized annealed importance sampling. *Phys. Rev. E*, 106(2):024127, 2022.
- [30] K. Cho, A. Ilin, and T. Raiko. Improved learning of gaussian-bernoulli restricted boltzmann machines. *In Proc. of the 21th International Conference on Artificial Neural Networks*, pages 10–17, 2011.
- [31] C. Takahashi and M. Yasuda. Mean-field inference in gaussian restricted boltzmann machine. *Journal of the Physical Society of Japan*, 85(3):034001, 2016.
- [32] M. Yasuda. Effective sampling on gaussian-bernoulli restricted boltzmann machines. *Nonlinear Theory and its Applications, IEICE*, 15(2):217–225, 2024.
- [33] M. Yasuda and K. Sekimoto. Gaussian–discrete restricted boltzmann machine with sparse-regularized hidden layer. *Behaviormetrika*, 2024.
- [34] F. E. Leonelli, E. Agliari, L. Albanese, and A. Barra. On the effective initialisation for restricted boltzmann machines via duality with hopfield model. *Neural Networks*, 143:314–326, 2021.